

# Diagrammatic Quantum Monte Carlo Algorithm in Momentum Representation: Hess-Fairbank Effect and Mesoscopics in 1D BEC with Attractive Interaction

P. F. Kartsev

*Department of Solid-State Physics, Moscow Engineering-Physics Institute  
(State University), Kashirskoe sh. 31, 115409 Moscow, Russia*

A novel algorithm of Diagrammatic Quantum Monte Carlo in momentum representation is reported in details. New models can be studied with this algorithm. For Bose systems with attractive interaction, the algorithm is free of the well-known minus-sign problem, while in other models it is weaker than in real-space methods.

Using this algorithm, we present the results of an exact numeric simulation of  $N$  one-dimensional bosons with attractive  $\delta$ -functional interaction in a rotating ring. We prove that in the large- $N$  limit the system can be described by conventional methods of weakly interacting gas, the dimensionless parameter of weak interaction being just  $1/N$ . When the strength of interaction is less than a certain threshold value, the dependence of angular momentum on the rotation frequency features plateaus characteristic of the irrotational fluid (the Hess-Fairbank effect).

PACS numbers: 03.75.Fi, 02.70.Ss, 68.65.-k

## I. QMC ALGORITHM IN MOMENTUM REPRESENTATION AGAINST SIGN PROBLEM

### A. Background: sign problem

The Quantum Monte Carlo (QMC) methods (variational, determinant, trajectory *etc.*) prove their usefulness for studying thermodynamics of diverse quantum systems. In QMC, the partition function  $Z = \text{Tr} e^{-\beta \hat{H}}$  is broken into series and summed using importance sampling. Each term is represented by unique set of inner parameters (MC configuration) and can be positive or negative depending on the actual MC configuration, the model Hamiltonian, and particle statistics. Alternating sign results in fluctuation of partition function and other quantities used in calculation. As the temperature is lowered, the errors grow larger making the calculation sluggish or even impossible. This is the so-called minus-sign problem, the inherent feature of most trajectory QMC methods.

Some cluster methods are free of minus sign. The determinant QMC method [1] is free of minus sign, but unfortunately, its application is restricted by fermionic and spin systems. Moreover, its running time as a function of cluster size  $L$  scales as  $L^3$  while in trajectory methods it is linear by  $L$ . So for large clusters, the expected slowing down of determinant method is stronger than that of trajectory method caused by sign problem. The method of exact diagonalization of Hamiltonian [2] is more useful and applies to wider class of models. Nevertheless, the size of system is limited by  $L_{\max} = 10 \div 12$  as the amount of needed calculations grows exponentially with increasing  $L$ .

Some sort of correction [3] makes possible to determine the ground-state energy with good precision even if approaching the temperature low enough is prevented by sign problem. For electrons on simple square (or cubic) lattice and hopping only to nearest neighbours, the

particle-hole transformation helps to remove part of sign not linked with Fermi statistics. But generally, sign problem is present in simulation.

This Letter is organized as follows. In Section I, we present the trajectory algorithm in momentum representation developed in the framework of Diagrammatic QMC method weakening or removing minus-sign in many models. In Section II, we study the one-dimensional bosonic system with attractive interaction in a rotating ring taken by Ueda and Leggett as a model of irrotational fluid [4]. This model can not be simulated with usual real-space methods, in part due to sign problem, while the algorithm described in this Letter is very efficient in this system allowing to simulate up to 100 and more particles.

### B. DQMC basics

In this paragraph, we repeat shortly the DQMC basics to be used later [5].

*Decomposition.* Diagrammatic QMC is based on the following decomposition of partition function into series of interaction representation:

$$Z = \sum_{m=0}^{\infty} \sum_{\{n^{(1)}\}} \int_0^{\beta} (-d\tau_{m-1}) \int_0^{\tau_{m-1}} (-d\tau_{m-2}) \dots \int_0^{\tau_1} (-d\tau_0) \times \\ \times e^{-\beta E_0^{(0)}} \prod_{j=1}^m e^{-\tau_j E_0^{(j-1)}} \left\langle \{n^{(j-1)}\} \right| \hat{V} \left| \{n^{(j)}\} \right\rangle e^{\tau_j E_0^{(j)}}, \quad (1)$$

where the system Hamiltonian is  $\hat{H} = \hat{H}_0 + \hat{V}$ , energies  $E_0(\dots)$  are given by  $\hat{H}_0$  which is chosen to be diagonal on occupation numbers  $\{n\}$ ,  $\tau_m \equiv \tau_0 + \beta$ ,  $\{n^{(m)}\} \equiv \{n^{(0)}\}$ ,

Each term in Eq. (1) is represented by its own picture of particle trajectories in  $(\mathbf{x}, \tau)$ -space, where  $\tau = 0 \div \beta$ ,

$\beta = 1/k_B T$ . The weight of a given MC configuration writes as

$$W_{\text{MC}} \sim \prod_{j=1}^m \left( -\Delta\tau \langle \dots | \hat{V} | \dots \rangle \exp(\dots) \right).$$

Then  $\tau_i$  mark the points of worldline distortions, the so-called “kinks” [5]. The imaginary-time step  $\Delta\tau$  can be taken small enough ( $\sim 10^{-8}\beta$ ).

*Process of calculation.* The importance sampling (Metropolis algorithm) consists in random transformations of MC configurations obeying the following requirements:

- *Full set.* Two arbitrary MC configurations with nonzero weight can be transformed into each other with nonzero probability and in finite number of steps;
- *Balance.* For each updating process transforming MC configurations A to B (“direct” process), we juxtapose the “inverse” process transforming MC configurations B exactly to A. Additionally, their frequencies must meet the balance equation

$$|W_A|P_{\rightarrow}p_{\rightarrow}^{(\text{acc})} = |W_B|P_{\leftarrow}p_{\leftarrow}^{(\text{acc})},$$

with  $W_A$  and  $W_B$  weights of MC configurations A and B,  $P_{\rightarrow}$  and  $P_{\leftarrow}$  the frequencies to call direct and inverse processes, and  $p_{\rightarrow}^{(\text{acc})}$  and  $p_{\leftarrow}^{(\text{acc})}$  the probabilities to accept the respective update. The latter are usually determined from the relations

$$\begin{aligned} p_{\rightarrow}^{(\text{acc})} &= \alpha, & p_{\leftarrow}^{(\text{acc})} &= 1, & \text{if } \alpha \leq 1, \\ p_{\rightarrow}^{(\text{acc})} &= 1, & p_{\leftarrow}^{(\text{rej})} &= 1/\alpha, & \text{if } \alpha > 1, \end{aligned}$$

where  $\alpha \equiv \left| \frac{W_B P_{\leftarrow}}{W_A P_{\rightarrow}} \right|$  is the so-called “acceptance ratio”. Therefore, to determine the probability of accepting the update, we must know parameters of respective inverse process.

There remain some freedom of choosing the time  $\tau$  of newly-created (or shifted) kink. The most reasonable approach is to choose  $\tau$  with probability  $\frac{\Delta\tau e^{-\delta E(\tau - \tau_{\min})}}{Z_1(\delta E, \tau_{\max} - \tau_{\min})}$  using relation

$$\tau = \tau_{\min} + P(\Delta E, \tau_{\max} - \tau_{\min}) \quad (2)$$

(see Appendix A), according to the fact that the weight of new MC configuration is proportional to  $e^{-\Delta E \tau}$ .

### C. DQMC in momentum representation

The algorithm described here is developed for systems with a Hubbard-like Hamiltonian in momentum representation

$$\hat{H} = \sum_p \epsilon_p \hat{a}_p^\dagger \hat{a}_p + \sum_{p,q,r,s} U_{pqrs} \hat{a}_p^\dagger \hat{a}_q^\dagger \hat{a}_r \hat{a}_s. \quad (3)$$

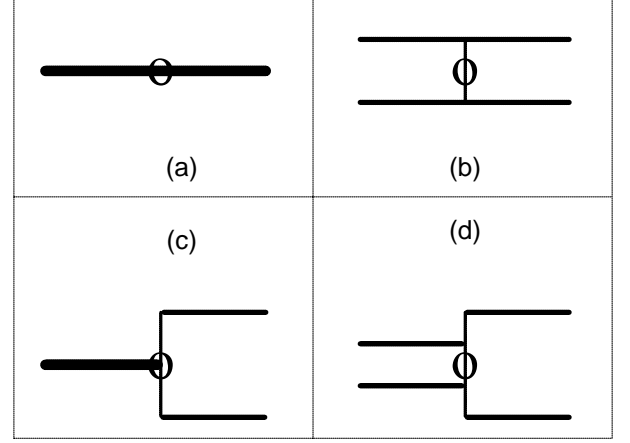


FIG. 1: Kinks generated by two-particle interaction: *a, b* – diagonal, *c, d* – non-diagonal; *a, b* in case of contact interaction  $U_{pqrs} = U_0 \delta_{p+q=r+s}$  can be taken into account analytically; *a, c* appear in simulation of Bose systems only. Here and throughout the paper, imaginary-time axis is plotted horizontally, momenta are placed vertically, occupation number indicated by line thickness.

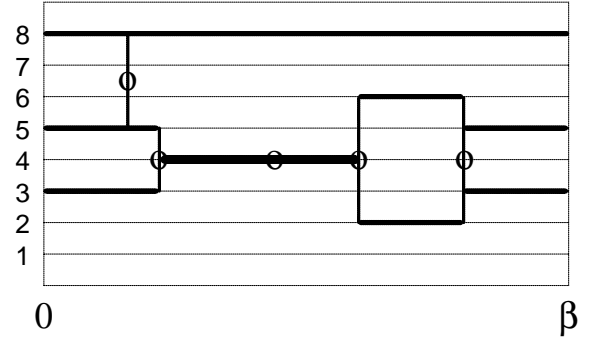


FIG. 2: Sample Monte Carlo configuration with all types of kinks.

Though typically, interaction term conserves full momentum  $U_{pqrs} = U_{pq} \delta_{p+q=r+s}$ , but it is not mandatory for this algorithm.

*Kinks.* The interaction term taken as a perturbation, generates four-ended kinks shown in Fig. 1. The multiplier entering the configuration weight due to each kink, is given by sum of respective  $U_{pqrs} \sqrt{n_p n_q n_r n_s}$  for all non-identical recombinations of momenta  $p, q, r, s$ . For Fermi systems, half of these terms get negative sign. This allows to use the standard relation  $\text{Sign}(F) = (-1)^{\sum_i (W_i^{(\tau)} - 1)}$  linking fermionic sign of configuration and time winding numbers  $W_i^{(\tau)}$  of worldlines which holds in real-space trajectory methods.

The example of MC configuration is sketched in Fig. 2.

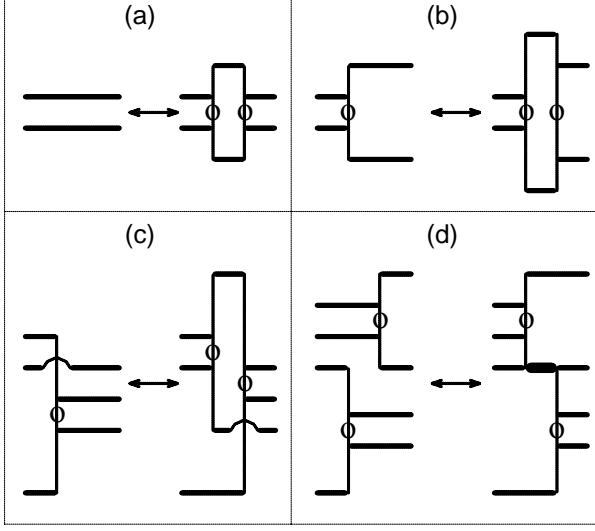


FIG. 3: The updating processes for non-diagonal kinks: Creation/Annihilation of Two Kinks (a), Expanding/Contracting of a Kink (b), Entangling of a Kink with a Worldline (c), and Shifting of a Kink Through Another (d).

*Sign problem.* The sign problem in usual real-space QMC algorithm is caused by hopping term. In this algorithm, on the contrary, it is caused by sign of interaction. Thus, weakly-interacting systems can be simulated in momentum representation with much greater precision.

For attractive interaction, the algorithm is free of sign problem, as every kink enters MC weight with positive factor. The particle-hole transformation for electrons on a lattice can remove part of sign not linked with Fermi statistics, in case when their interaction is  $\sum_{ij} V_{ij} n_{i\uparrow} n_{j\downarrow}$ .

In simple but rather wide case of point interaction  $U_{pqrs} = U_0 \delta_{p+q, r+s}$ , the diagonal part of interaction (kinks Fig. 1 (a,b)) is summed analytically and the MC configurations with single kink giving most part of sign problem, become impossible. Monte Carlo weight can become negative for three and more kinks, but in lower orders by  $\beta U$  all diagrams are positive-definite with no relation to particle statistics. As a result, the system can be simulated at lower temperature.

*Updates.* The processes chosen to update worldline configuration, are shown in Fig. 3. In addition, the time-shifting of kink should be used to speed-up calculation. For subsystem of diagonal kinks, their creation/annihilation and time-shifting are enough.

Note, in case of momentum conservation  $p + q = r + s$  these processes can not change full momentum  $K$  of the system. As a result, the calculation is done in the sector of phase space with fixed  $K$ . This situation can be corrected by introducing fictitious kinks changing number

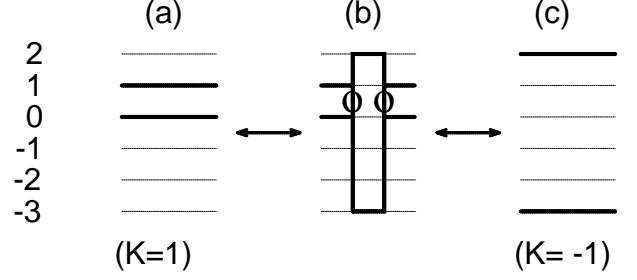


FIG. 4: Creation of two “biased” kinks and annihilation of them in different way change full momentum of the system.

of particles ( $\eta \sum_i (\hat{a}_i + \hat{a}_i^+)$ , like in Worm algorithm[6]), or full momentum ( $\eta \sum_{\substack{pqrs \\ p+q \neq r+s}} \hat{a}_p^+ \hat{a}_q^+ \hat{a}_r \hat{a}_s$ , see Fig. 4), with  $\eta$  small enough. However, fictitious kinks are not needed when calculating energy levels characterized by their own value of full momentum.

#### D. Applications of the method

*1D Fermi Hubbard model.* In testing purposes, we used the algorithm to calculate the ground state of the one-dimensional fermionic system with the Hamiltonian  $\hat{H} = t \sum_{\langle ij \rangle \sigma} (\hat{a}_{i\sigma}^+ \hat{a}_{j\sigma} + H.c.) + U \sum_i \hat{n}_{i\uparrow} \hat{n}_{i\downarrow}$  with  $t=1$ ,  $U=-1$ , length of the chain  $L = 8$ ,  $K = 0$ , number of particles  $N_{\uparrow} = N_{\downarrow} = 4$ . The result  $E_0 \simeq -11.9523$  was checked with exact diagonalization ( $E_0 = -11.952326$ ) and real-space Worm algorithm.

The average sign for both QMC algorithms as a function of  $\beta$  is shown in Fig. 5. The graph confirms our assumption that sign problem is much weaker in new algorithm even for Fermi systems. With new algorithm, the maximal possible value of  $\beta$  in sample system is increased from 7 to 40.

It is worthy to note that such rather good precision of 5 digits became possible because of fixation of full momentum  $K = 0$ . The second energy level  $E_1 = -11.901727$  corresponding to  $K \neq 0$  is extremely close to the ground state, so the precision of real-space QMC is limited by 3 digits as lowering of the temperature is prevented by sign problem.

*Fractional Quantum Hall Effect.* In studying Wigner Crystallization in Fractional Quantum Hall Effect, the fermionic Hamiltonian of view (3) was obtained and then analysed using exact diagonalization method [7]. Now the QMC algorithm described here, was applied to this system in order to confirm or deny the existence of Wigner crystal. Unfortunately, the fermionic sign problem appeared too strong to determine the ground-state properties in this model.

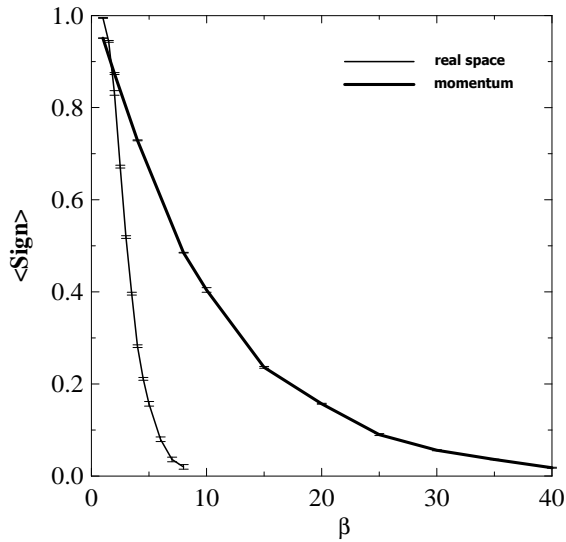


FIG. 5: Average sign of MC configuration as a function of  $\beta = 1/k_B T$  for QMC calculations of the 1D Fermi Hubbard model with  $L = 8$  sites,  $N_\uparrow = N_\downarrow = 4$ ,  $U = -1$ ,  $t = 1$ , in both real space and momentum representations. The calculations become impracticable for  $\langle \text{Sign} \rangle < 0.01$ , so with momentum representation (and fixed full momentum  $K = 0$ )  $\beta_{\text{max}}$  increases from 7 to 40.

*Bose gas with attraction in a box.* The best model for the algorithm described in this Letter is a Bose gas in a box with attractive interaction. In addition to the freedom of sign problem, this algorithm gets more advantage here, as the model can not be simulated by real-space QMC without errors [8]. These are caused by discretization of continuous real space needed to apply lattice QMC methods.

## II. ROTATING BOSE-EINSTEIN CONDENSATE WITH ATTRACTIVE INTERACTION IN ONE DIMENSION: HESS-FAIRBANK EFFECT AND MESOSCOPICS

### A. Background: macroscopic study

Recent remarkable progress in Bose-Einstein condensation of dilute alkali gases [9] has opened up an opportunity of studying delicate quantum phenomena in ultra-cold multi-atomic systems. One of intriguing set-ups is a system of (quasi)-one-dimensional (1D) bosons with attractive interaction – like  $^7\text{Li}$  – in a rotating ring [4, 10]. In contrast to 3D case, where the Bose-Einstein condensate of attracting atoms becomes unstable with respect to a collapse [11] above a certain threshold [which decreases (vanishes) with decreasing (vanishing) the trapping potential], the 1D system is unconditionally stable even without the trapping potential, though in a latter case it forms a droplet (see, e.g., [12]).

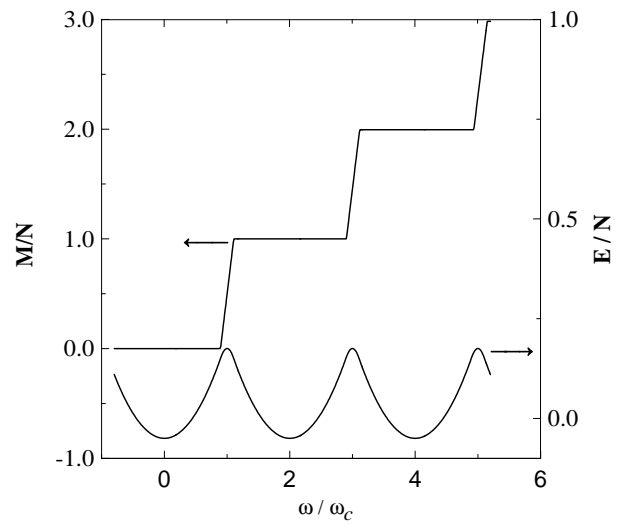


FIG. 6: Dependence of the groundstate energy  $E$  (lower curve) and angular momentum  $M$  (upper curve) on the rotation frequency  $\omega$ .  $\gamma = 0.1$ ,  $N \rightarrow \infty$ .

Ueda and Leggett [4] have risen a question of whether the system of 1D attractive bosons in a finite-size rotating toroidal trap can remain irrotational, that is demonstrate the behavior typical for a superfluid – the so-called Hess-Fairbank (HF) effect [13]. On the basis of their (approximate) treatment, they arrived at the conclusion that the HF effect should take place in the system, provided the strength of interaction is below a certain threshold value. However, recently Berman *et al.* [10] have questioned this result, arguing that the HF effect disappears at arbitrarily small value of attractive interaction due to a specific quantum instability.

In this Section, we resolve the above-mentioned controversy by an exact numeric study of  $N$  rotating 1D bosons with the  $\delta$ -functional attractive interaction. We do observe the HF effect predicted by Ueda and Leggett (though the threshold interaction differs by a factor of 2 from the value found in Ref. [4]). Moreover, our data clearly demonstrate that in the large- $N$  limit the conventional methods of weakly interacting Bose gas – like Gross-Pitaevskii (GP) equation [14] and Bogoliubov technique [15] – become applicable, the dimensionless small parameter controlling the accuracy of the approximation being just  $1/N$ . The classical-field language of GP equation renders the issue of the presence and disappearance of the HF effect especially transparent. The effect persists as long as the condensate density remains uniform, and disappears with breaking the spatial homogeneity of the condensate. In a few particle system, the deviations from the mean-field picture are significant. In particular, with decreasing  $N$  the HF effect gradually becomes indistinguishable from the generic effects of angular momentum quantization.

Consider  $N$  bosons of the mass  $m$  placed in the ro-

tating torus of radius  $R$  and cross-sectional area  $S = \pi r^2$ . At low enough temperature and with the condition  $r \ll R$  met, the system is quasi-one-dimensional, and the effective 1D Hamiltonian in the rotating (with angular frequency  $\omega$ ) frame reads

$$H = \sum_k \left(k - \frac{\omega}{2}\right)^2 n_k + \frac{g}{2} \sum_{k,l,q} a_k^+ a_l^+ a_{l-q} a_{k+q}, \quad (4)$$

where the integers  $k, l, q$  stand for angular momenta,  $a_k^+$  creates a boson with angular momentum  $k$ ,  $n_k = a_k^+ a_k$ ;  $g = 2a/mRS$  (with  $a < 0$  the 3D scattering length) is the effective vertex of pair interaction; we use units  $\hbar = 1$  and  $\omega_c = 1$ , where  $\omega_c = 1/2mR^2$  is the critical rotation frequency equal to the period of variation of the groundstate energy as a function of  $\omega$ . The groundstate of the system is defined by the three parameters,  $N$ ,  $\gamma = |g|(N-1)$ , and  $\omega$ .

Ueda and Leggett [4] have analyzed the model (4) in the Hartree-Fock approximation in the Fock basis of angular momentum eigen states  $\{|\dots, n_{-1}, n_0, n_1, \dots\rangle\}$ . They argued that in the limit of  $\gamma \rightarrow 0$ , when no more than two single-particle angular momentum eigen modes survive, their approximation is superior with respect to the other treatments of weakly interacting bosons. A typical result for  $\gamma \ll 1$  is shown in Fig. 6. The HF effect – plateaus in the angular momentum curve,  $M(\omega)$ , – takes place almost at any  $\omega$ , except for a close vicinity of the critical frequency  $\omega_c$ . With increasing  $\gamma$ , the size of the plateaus gets smaller, and the HF effect completely disappears at some critical point  $\gamma = \gamma_c \sim 1$ . At this point we note that  $\gamma_c$  cannot be found accurately with the treatment of Ref. [4], because more than two single-particle angular momentum eigen modes are involved in the formation of the groundstate. This is immediately seen from the *variational* Hartree-Fock treatment, when all the particles are placed into one and the same spatially dependent single-particle state  $\psi_0(x)$  (non-uniform Bose-Einstein condensate), the wavefunction  $\psi_0(x)$  being defined from the minimal energy condition, which leads to the GP equation

$$(i\partial/\partial x + \omega/2)^2 \psi_0 - 2\pi\gamma|\psi_0|^2\psi_0 - \mu\psi_0 = 0, \quad (5)$$

where  $\mu$  is taken to satisfy the normalization condition  $\int |\psi_0(x)|^2 dx = 1$ . Solving Eq. (5) reveals the nature of the HF effect, as well as the mechanism of its disappearance. At  $\omega \leq \omega_*(\gamma)$ , with  $\omega_*(\gamma)$  satisfying

$$(\omega_* - 2k)^2 = 1 - 2\gamma, \quad (6)$$

the solution  $\psi_0(x)$  is uniform and thus irrotational. At  $\omega > \omega_*(\gamma)$ , the rotational symmetry of the problem breaks down: The density becomes non-uniform, and the rotation of the density profile gives rise to the increase of the angular momentum with growing  $\omega$ . At  $\gamma > \gamma_c = 1/2$  the minimal-energy solution is non-uniform even without the rotation [16], and the HF effect totally disappears.

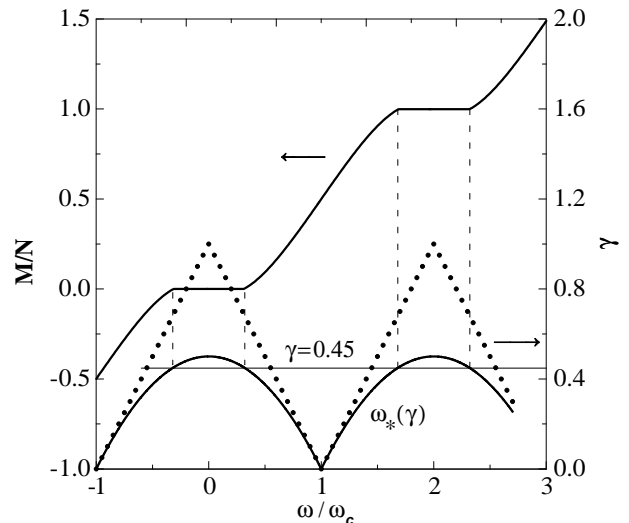


FIG. 7: Function  $M(\omega)$  at  $\gamma = 0.45$ , as predicted by GP equation (upper solid curve). Lower solid curve represents  $\omega_*(\gamma)$ , according to Eq. (6). Dotted curve is the prediction of Ref. [4] for  $\omega_*(\gamma)$ .

A simple and instructive way of arriving at the relation (6) is the Bogoliubov treatment [15] for the elementary excitation spectrum in assumption of the uniform condensate. Considering the energy,  $\epsilon_1$ , of the first excited state, one observes that at  $\omega > \omega_*$ , the uniform condensate is *thermodynamically* unstable:  $\epsilon_1 < 0$ . At  $\gamma > 1/2$  the energy  $\epsilon_1$  becomes imaginary, indicating *dynamical* instability of the homogeneous solution at any  $\omega$ .

At  $\gamma \gg 1$  the solution of Eq. (5) is strongly non-uniform and corresponds to a rotating condensate droplet – bright soliton [17, 18].

To obtain the GP prediction for the angular momentum as a function of  $\omega$ , we solved Eq. (5) by numerically minimizing GP energy functional, see Figs. 7, 8. At  $\gamma \ll 1$ , the GP results coincide, up to higher-order corrections, with those of Ref. [4]. At  $\gamma \sim 1$ , however, deviations become significant.

## B. Simulation for finite $N$

As we have already mentioned, the very existence of the HF effect (and thus the applicability of the weakly interacting gas treatments) has been questioned recently by Berman *et al.* [10]. This conclusion of Ref. [10] seems rather strange and counter-intuitive in view of the known exact results for the 1D attractive bosons in the non-restricted geometry. The small parameter that guarantees applicability of the mean-field approach is just the inverse number of particles [12]. *A priori* we do not see how the finite system size can qualitatively change the situation.

In view of this controversy, as well as keeping in mind

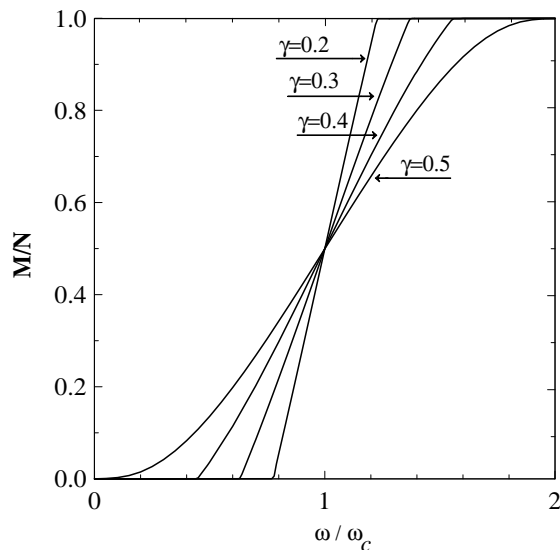


FIG. 8: Gross-Pitaevskii equation results for the function  $M(\omega)$  at different  $\gamma$ 's.

the fact that mesoscopic results are interesting in their own value, we performed an exact numeric study of the model (4) for different numbers of bosons.

Analytic summation of diagonal kinks contribution due to point interaction  $U_{pqrs} = U_0\delta_{p+q,r+s}$  increases full energy by constant  $\Delta E = U_0(2N^2 - N)$ , and particle energy obtains term depending on occupation  $\tilde{\epsilon}_k = (k - \omega/2)^2 - U_0n_k$ .

After typical update, the weight of MC configuration acquires the factor  $\sim e^{-\delta E(\tau - \tau_0)}$ . Main difference from lattice models is that  $\delta E$  can be unlimitedly large, so with large  $\delta E$ , the weight of new configuration would be too small to appear in simulation and the efficiency of the update approaches zero. Therefore we must choose for update different places with different probability to make simulation effective enough.

Note, for old  $\epsilon_k = (k - \omega/2)^2$ , there exist simple relation  $\delta E = 2q(q + \Delta)$  with  $\Delta$  characterizing the place of update. Therefore we can neglect second term  $-U_0n_k$  in new particle energy  $\tilde{\epsilon}$ , and choose  $q$  using simple analytics, given in Appendix B for all types of updates. Though for small  $k$ , both terms in new particle energy  $\tilde{\epsilon}_k$  are comparable (for in this model  $U_0 = \gamma/2(N - 1)$ ,  $\gamma \leq 1$ ), this trick is aimed mostly for reasonable choosing of large momentum  $k$  where  $\langle n_k \rangle \simeq 0$  making second term rather virtual.

### C. Results

We traced the evolution of the system properties with  $N$  varying from 2 to 100, at different  $\omega$ 's and  $\gamma$ 's. The simplest characteristics that we studied was the groundstate energy, which we calculated by simulating the groundstates in different angular momentum sectors,

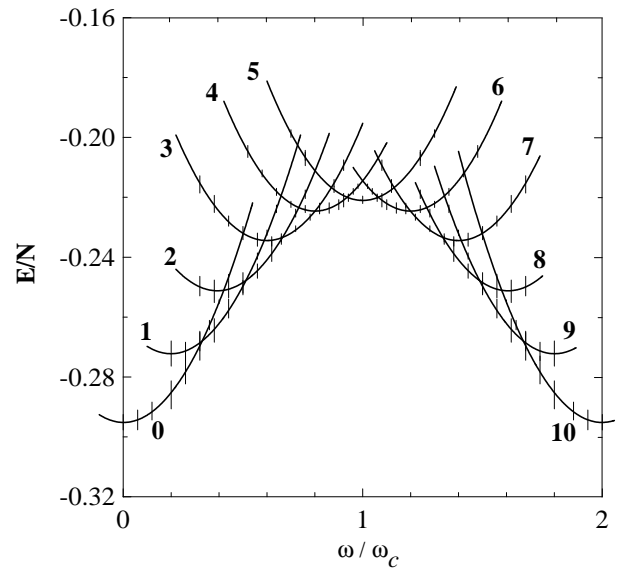


FIG. 9: Groundstate energies in different angular momentum sectors for  $N = 10$  at  $\gamma = 1/2$ . The bars are the Monte Carlo data with errors. The solid curves are the parabolic fits. Integers stand for the values of the angular momenta.

with subsequent selecting the global minimum, see Fig. 9. This procedure yields also the curve  $M(\omega)$ . For a finite- $N$  system this curve is essentially stepwise due to the quantization of angular momentum. Comparing this curve at large enough  $N$  to the Gross-Pitaevskii solution, we find an excellent agreement, see Fig. 10.

To quantitatively trace the difference between GP and Monte Carlo results, we compared corresponding answers for the groundstate energies at different  $N$ 's. We found that starting from  $N \approx 10$  the deviation between the two results scales as  $1/N$ , which confirms that in the  $N \rightarrow \infty$  limit the Gross-Pitaevskii equation yields a perfect description of the groundstate properties.

In Fig. 11 we present the  $M(\omega)$  curves for  $\gamma = 0.2 < \gamma_c = 1/2$ , at different particle numbers. Once again we see an excellent agreement with the GP equation at large  $N$ . The HF plateau is unambiguously revealed. Note, that at  $N \lesssim 5$  the HF plateau at zero momentum is indistinguishable (by its size) from the rest of the quantized-momentum plateaus.

To get an insight into the inner structure of the ground state, we calculate the two-particle density correlator  $K(x) = \langle \Psi^\dagger(x')\Psi^\dagger(x'+x)\Psi(x'+x)\Psi(x') \rangle_{x'}/N(N-1)$ . In Figs. 12 and 13 we present  $K(x)$  ( $\omega = 0$ ) for  $\gamma_1 = 0.25$  and  $0.75$ , that is for uniform and non-uniform (in the macroscopic limits) cases, respectively. At small enough  $N$  there is no qualitative difference between the two cases. At large  $N$  the difference is clearly seen. Once again note an excellent agreement with the GP equation.

Summarizing, we developed a novel Quantum Monte Carlo algorithm based on the generic principles of the Diagrammatic Monte Carlo approach [5]. The algorithm

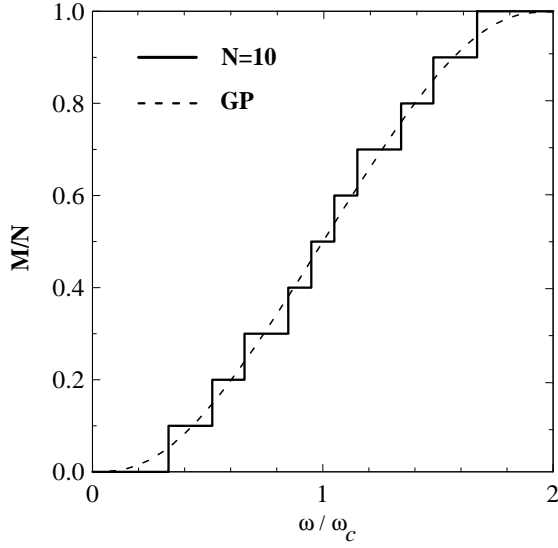


FIG. 10: Groundstate angular momentum  $M$  as a function of the rotation frequency  $\omega$  for  $N = 10$  at  $\gamma = 1/2$  (solid line). Absolute error is on the order of  $10^{-2}$ . Dotted curve is the  $N \rightarrow \infty$  limit obtained by solving Gross-Pitaevskii equation.

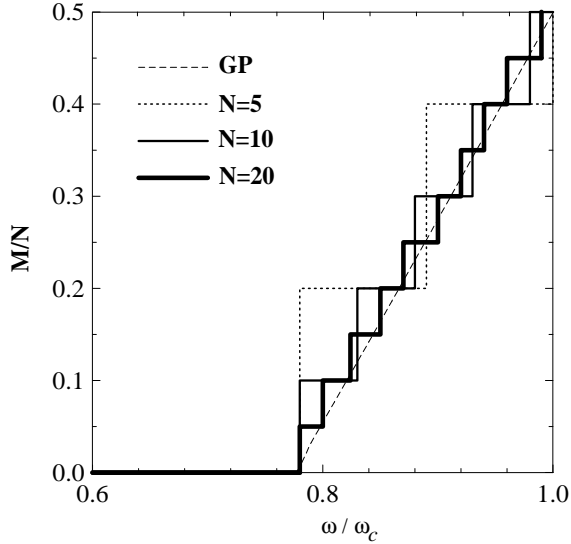


FIG. 11: Groundstate angular momentum  $M$  as a function of rotation frequency  $\omega$  for  $N = 5, 10, 20$  at  $\gamma = 0.2 < \gamma_c = 1/2$ . Absolute error is on the order of  $10^{-2}$ . The dashed line is the result of the Gross-Pitaevskii equation.

samples exact diagrammatic expansion (in terms of the pair interaction) of the imaginary-time evolution operator in the *momentum* representation. In comparison with usual real-space methods, this algorithm is more efficient in simulation of weakly interacting systems. Moreover, it can be applied to the models which can not be studied by real-space methods. The sign problem is weaker

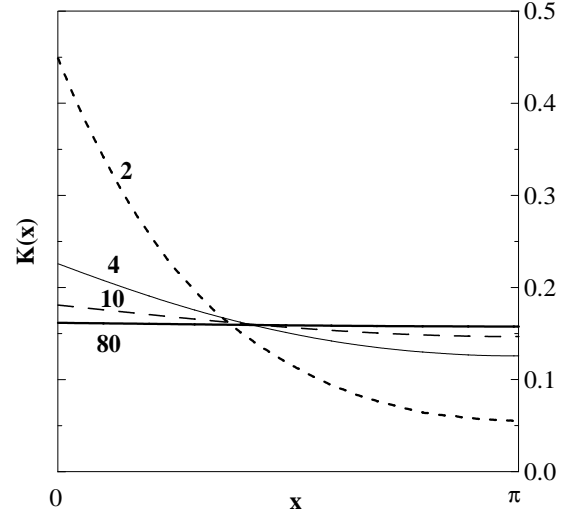


FIG. 12: Density-density correlator  $K(x)$  ( $\omega = 0$ ) at  $\gamma = 0.25 < \gamma_c = 1/2$  for  $N = 80, 10, 4, 2$ . The correlations grow up with decreasing  $N$ .

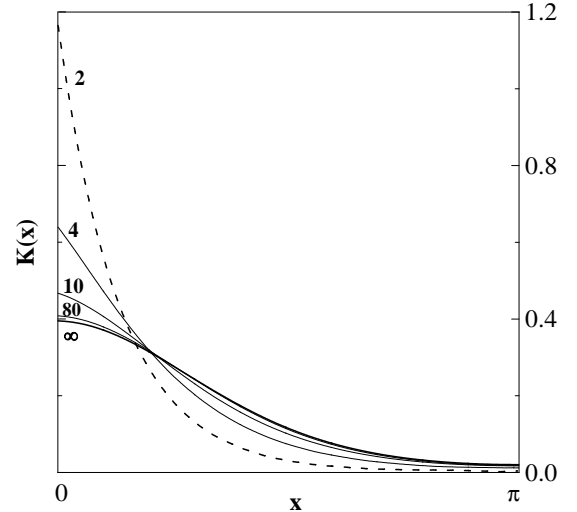


FIG. 13: Density-density correlator  $K(x)$  ( $\omega = 0$ ) at  $\gamma = 0.75 > \gamma_c = 1/2$  for  $N = 80, 10, 4, 2$ . Solid curve corresponds to the Gross-Pitaevskii equation. The particle positions are correlated even in the macroscopic limit indicating the non-uniformity of the groundstate.

here making possible to reach temperatures low enough to study ground state. In the case of attractive pair potential, all diagrams are positive-definite and the method is very efficient, allowing to simulate up to 100 and more particles.

Using exact Quantum Monte Carlo algorithm, the groundstate properties of one-dimensional bosons with attractive  $\delta$ -functional interaction in a rotating toroidal trap are studied. The Hess-Fairbank effect – absence of

a response to the trap rotation – is observed in a certain area of the parameter space. The fact that in the  $N \rightarrow \infty$  limit the Gross-Pitaevskii equation yields a perfect description of the groundstate properties is proved.

The author is grateful to Profs. V.A. Kashurnikov, B.V. Svistunov, and N.V. Prokof'ev for drawing my attention to this problem and numerous helpful discussions. This work was supported by the Russian Foundation for Basic Research.

## APPENDIX A: WEIGHTING THE TIME OF NEW KINK

With adding new kink in time  $\tau$  in range  $(\tau_{min} \dots \tau_{max})$ , the statistical weight of MC configuration receives a factor  $\sim e^{-Q(\tau - \tau_{min})}$ , where  $Q$  denotes change of worldline energy in the range  $(\tau_{min} \dots \tau)$  after update.

Time  $\tau$  is determined with probability  $\Delta\tau \frac{e^{-Q(\tau - \tau_{min})}}{Z_1(Q, \tau_{max} - \tau_{min})}$  using relation

$$\tau = \tau_{min} + P(Q, \tau_{max} - \tau_{min}, R),$$

where  $R$  is the random number uniformly distributed between 0 and 1.

For convenience, we define the following functions:

$$Z_1(Q, T) = \begin{cases} \frac{e^{-QT} - 1}{-Q}, & \text{usually,} \\ T, & \text{if } |Q| \rightarrow 0, \\ \frac{1}{Q}, & \text{if } Q \rightarrow +\infty, \\ \frac{e^{-QT}}{-Q}, & \text{if } Q \rightarrow -\infty, \end{cases} \quad (A1)$$

$$P(Q, T, R) = \begin{cases} -\frac{\ln(1 + R(e^{-QT} - 1))}{Q}, & \text{usually,} \\ RT, & \text{if } |Q| \rightarrow 0, \\ \frac{1}{Q} \ln R, & \text{if } Q \rightarrow +\infty, \\ T - \frac{1}{|Q|} \ln R, & \text{if } Q \rightarrow -\infty. \end{cases} \quad (A2)$$

Limiting cases should be realized separately to avoid algorithm inefficiency and precision loss.

## APPENDIX B: UPDATES IN DETAILS

### a. Creation/Annihilation of Two Kinks

This process is shown in Fig. 14.

Two kinks are created as follows:

1. Time of first kink  $\tau_0$  from 0 to  $\beta$  is chosen in random way with probability  $\frac{\Delta\tau}{\beta}$ .
2. Two not-empty world lines are found going through  $\tau_0$  with momenta  $k_1$  and  $k_2$ , including possible case  $k_1 = k_2$ . Let us denote the probability to choose these world lines  $W(k_1, k_2)$ .

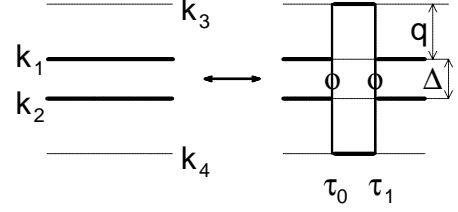


FIG. 14: Creation/Annihilation of Two Kinks.

3. The second kink will be created at the time  $\tau_1$  determined using Appendix A.

$$\tau_1 = \tau_0 + P(2q(q + \Delta), \tau_{max} - \tau_0).$$

With increasing  $k_3$  and  $k_4$ , their average occupation becomes exponentially small, so  $\tau_{max}$  remains intact. This fact allows us to take into account all possible  $k_3, k_4$  in single process. The analytics for choosing  $q$  is given in Appendix C,

4. The probability to accept this process is found from the balance equation (B1).

The scheme of annihilation:

1. A random kink having parameters  $\tau_0, k_1, k_2, q, U_{eff}, n_{eff}$  is taken with probability  $\frac{1}{Q_{new}} = \frac{1}{Q_{old} + 2}$ .
2. The kink chosen and its right neighbour (the direction is fixed to remove polyvalence) must form the “kink-antikink” pair.
3. The probability to choose  $q$  in the direct process is  $\frac{W(q)}{Z_3}$ .
4. The annihilation probability  $p_{\leftarrow}^{(acc)}$  of this pair is determined from the balance equation (B1).

$$W_{old} W(k_1, k_2) \frac{W(q)}{Z_3} \frac{\Delta\tau}{\beta} \frac{\Delta\tau e^{(\dots)}}{Z_1} p_{\rightarrow}^{(acc)} = \quad (B1)$$

$$W_{old} (-\Delta\tau U_{eff} n_{eff})^2 e^{(\dots)} \frac{1}{Q + 1} p_{\leftarrow}^{(acc)}.$$

(Pay attention to the possibility of pair annihilation in two different ways when all four momenta  $k_1, \dots, k_4$  are untouched by other kinks, see Fig. 15. To remove this duality we disable the annihilaton when  $\tau_1 < \tau_0$ ).

### b. Kink Expanding/Contracting - particle version

The direct process (see Fig. 16) is done as follows:



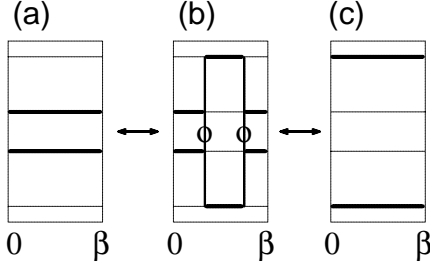


FIG. 15: About possibility to annihilate a pair of kinks in two ways resulting in different configurations.

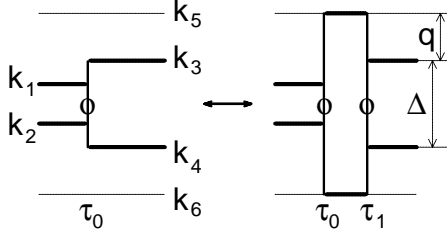


FIG. 16: Process of Kink Expanding/Contracting - particle version.

1. A random kink having parameters  $\tau_0, k_1, \dots, k_4, U_1, n_1$  is chosen with probability  $\frac{1}{Q}$ .
2. Choice of  $q$  and  $\tau_1$  is done similarly to the creation of two kinks with probabilities  $W(q)/Z_3$  and  $\exp(-\Delta E(\tau_1 - \tau_0))/Z_1$ , respectively.
3. The probability to accept this update is determined using balance equation (B2).

Inverse transformation:

1. A random kink having parameters  $\tau_0, k_1, \dots, k_4, U_2, U_3, n_2, n_3$  is chosen with probability  $\frac{1}{Q_{new}} = \frac{1}{Q_{old} + 1}$ .
2. The kink chosen must, with its right neighbour, form the pair which can be contracted into single kink.
3. The probability to choose this  $q$  in direct process equals  $W(q)/Z_3$ .
4. The probability to accept this update is determined from the balance equation (B2).

$$W_{common}(-\Delta\tau U_1 n_1) \frac{1}{Q} \frac{W(q)}{Z_3} \frac{\Delta\tau e^{(\dots)}}{Z_1} p_{\rightarrow}^{(acc)} = \quad (B2)$$

$$W_{common}(-\Delta\tau)^2 U_2 U_3 n_2 n_3 e^{(\dots)} \frac{1}{(Q+1)} p_{\leftarrow}^{(acc)}$$

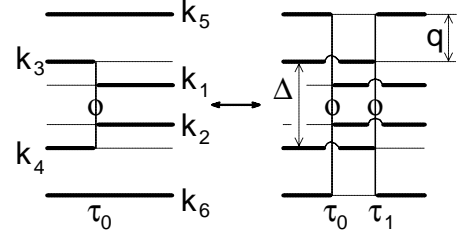


FIG. 17: Kink Expanding/Contracting - "hole" version.

### c. Kink Expanding/Contracting - "hole" version

In contrast to previous update, this process needs momenta  $k_5, k_6$  to be occupied. However, in each moment  $\tau_0$  only limited set of occupied pairs  $(k_5, k_6)$  exists with  $k_5 + k_6 = k_1 + k_2$  (see Fig. 17), i.e. fitting this update. Therefore the momenta should not be weighted using formulas of Appendix C. Otherwise, we choose a random pair from rather small set.

The direct update is made as follows:

1. A random kink having parameters  $\tau_0, k_1, \dots, k_4, U_1, n_1$  is chosen with probability  $\frac{1}{Q}$ .
2. All pairs  $(k_5, k_6)$  fitting this process are determined; for each pair, the parameters  $\tau_{max}, n_2, n_3, U_2, U_3, \Delta E$  are found.
3. Each pair  $(k_5, k_6)$  is chosen with probability  $W(k_5, k_6) \sim U_2 U_3 n_2 n_3 Z_1(\Delta E, \tau_{max} - \tau_0)$ ;
4. The balance equation (B3) is used to determine the probability to accept this update.

The inverse process is made as follows:

1. A random kink having parameters  $\tau_0, k_1, k_2, k_5, k_6, U_2, U_3, n_2, n_3$  is chosen with probability  $\frac{1}{Q_{new}} = \frac{1}{Q_{old} + 1}$ .
2. The kink chosen and its right neighbour must form the pair which can be contracted into single kink fitting the direct "hole" update.
3. The probability  $W(k_5, k_6)$  to choose this pair  $(k_5, k_6)$  in direct process, is determined.
4. The probability to accept this update is determined from the balance equation (B3).

$$W_{common}(-\Delta\tau U_1 n_1) \frac{1}{Q} W(k_5, k_6) \frac{e^{(\dots)}}{Z_1} p_{\rightarrow}^{(acc)} = \quad (B3)$$

$$W_{common}(-\Delta\tau)^2 U_2 U_3 n_2 n_3 e^{(\dots)} \frac{1}{(Q+1)} p_{\leftarrow}^{(acc)}$$

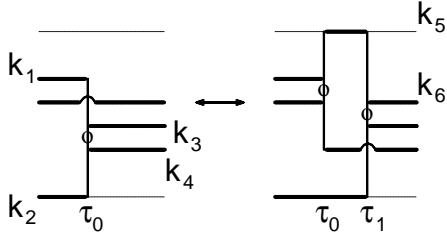


FIG. 18: Entangling of a Kink with a Worldline. In the case shown here, the upper parts of left and right kinks are touched.

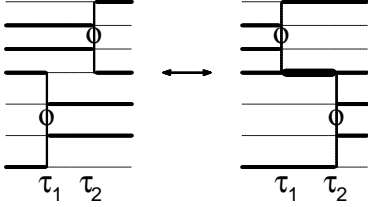


FIG. 19: Shifting the Kink Through Another. Kinks exchange their times; the occupation numbers are changed for worldlines with momenta common for both kinks.

#### d. Entangling of a Kink with a Worldline

This process can not be made of the processes described above. More visually, this is the only process able to change the winding numbers of worldlines. There exist many versions of this update. The case touching upper parts of left and right kinks is shown in Fig. 18,

The momentum  $k_6$  should be occupied at  $\tau_0$ , thus there is only limited set of pairs  $(k_5, k_6)$  fitting the process of entangling. Therefore, the schemes of direct and inverse updates are similar to that for the previous transformation. The only correction should be made is to choose upper or lower parts of kinks, if present.

#### e. Shifting the Kink Through Another

Carrying out shift in time, one must take into account possible collisions with neighbouring kinks. While simple shift is enough for simulating Fermi systems, Bose case should incorporate shift "through" neighbouring kink (Fig. 19). In this process, the kinks are exchanged by time:  $\tau_2^{new} = \tau_1^{old}$ ,  $\tau_1^{new} = \tau_2^{old}$ .

The number  $K$  of common momenta can be 1 to 4. The case  $K = 4$  is usually associated with the "kink-antikink" pair, so the shifting through the kink can be replaced by the combination of Annihilation and Creation. However, another case shown in Fig. (20) can appear in simulation of Bose chain.

Due to symmetry, direct and inverse processes are iden-

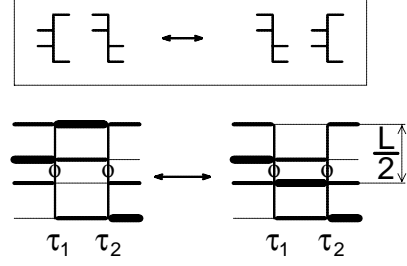


FIG. 20: To the process of Shifting the Kink Through Another. In simulation of periodical chain, two kinks can occupy all the same momenta though not forming the "kink-antikink" pair.  $L$  denotes the length of a chain.

tical. The scheme is as follows:

1. A random kink having parameters  $\tau_0, k_1, \dots, k_4$  is chosen with probability  $\frac{1}{Q}$ ;
2. The nearest kink on the right with at least one the same momentum, is found;
3. The parameters  $\Delta E_{before}, \Delta E_{after}, n_{before}, n_{after}$  are determined;
4. The probability to accept the update is determined from the balance equation (B4).

$$W_{common} U_1 U_2 n_{before} e^{-\Delta E_{before}(\tau_2 - \tau_1)} \frac{1}{Q} p_{\rightarrow}^{(acc)} = \quad (B4)$$

$$W_{common} U_1 U_2 n_{after} e^{-\Delta E_{after}(\tau_2 - \tau_1)} \frac{1}{Q} p_{\leftarrow}^{(acc)},$$

or, finally,

$$\alpha \equiv \left| \frac{p_{\rightarrow}^{(acc)}}{p_{\leftarrow}^{(acc)}} \right| = \frac{n_{after}}{n_{before}} e^{-(\Delta E_{after} - \Delta E_{before})(\tau_2 - \tau_1)}.$$

### APPENDIX C: CHOOSING MOMENTUM ANALYTICALLY

We use the fact  $\delta E = 2q(q + \Delta)$ , where  $\Delta$  is fixed in choosing the place of action, and  $q > -\Delta/2$ . The value of  $Z_1(\delta E(q), T)$  as a function of  $q$ , is shown in Fig. 21. It can be approximated by following piecewise function

$$Z_1 \approx W(q) = \begin{cases} Z_1(E(q), T), & \text{if } q < 0 \\ const = T, & \text{if } 0 < q \leq q^*, \\ \frac{1}{E(q)}, & \text{if } q > q^*, \end{cases} \quad (C1)$$

making possible to determine  $q$  analytically.

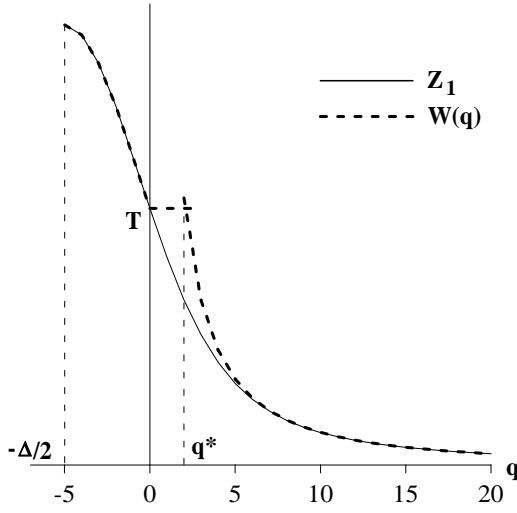


FIG. 21:  $Z_1(T, 2q(q + \Delta))$  as a function of  $q$  (solid curve) and its piecewise approximation  $W(q)$  (dotted curve) used to choose  $q$  analytically.

The choice of  $q^*$  is based on the relation  $1/E(q^*) \approx T$ :

$$q^* = \begin{cases} \sqrt{\frac{1}{2T}}, & \text{if } \Delta = 0, \\ \frac{\Delta}{2} \left( \sqrt{1 + \frac{2}{T\Delta^2}} - 1 \right), & \text{if } \Delta > 0. \end{cases} \quad (\text{C2})$$

The possibility to choose given  $q$  equals  $\frac{W(q)}{Z_3}$  where  $Z_3 = Z^{(-)} + Z^{(0)} + Z^{(+)}$ , and

$$Z^{(-)} = \sum_{q=q_{\min}}^{-1} W(q), \quad (\text{C3})$$

$$Z^{(0)} = \sum_{q>0}^{q^*} T = Tq^*, \quad (\text{C4})$$

$$Z^{(+)} \simeq \sum_{q>q^*}^{\infty} \frac{1}{2q(q + \Delta)} \simeq \begin{cases} \frac{1}{2q^*} & \text{if } \Delta = 0, \\ \frac{1}{\Delta} \ln \left( 1 + \frac{\Delta}{q^*} \right) & \text{if } \Delta > 0 \end{cases} \quad (\text{C5})$$

correspond to three pieces of approximation (C1). Values  $Z^{(-)}$ ,  $Z^{(0)}$ ,  $Z^{(+)}$  define boundary values  $R^{(-)} = \frac{Z^{(-)}}{Z_3}$  and  $R^{(+)} = 1 - \frac{Z^{(+)}}{Z_3}$ .

To choose  $q$ , the random number  $R$  uniformly distributed between 0 and 1. is taken. Initially, we determine the range ( $q < 0$ ,  $0 < q \leq q^*$ ,  $q > q^*$ ), then  $q$  according to the range found. When  $R \leq R^{(-)}$ , we find the value  $q < 0$ , making  $\sum_{q'=q_{\min}}^{q'<q} W(q')$  greater than  $RZ_3$ .

Other cases allow analytical relation:  $q = 1 + q^* \frac{R - R^{(-)}}{R^{(+)} - R^{(-)}}$  if  $R^{(-)} < R \leq R^{(+)}$ , and

$$q = \begin{cases} \frac{q^*}{r}, & \Delta = 0, \\ \frac{\Delta}{(1 + \Delta/q^*)^r - 1}, & \Delta > 0, \end{cases}$$

where  $r = \frac{R - R^{(+)}}{1 - R^{(+)}}$ , if  $R > R^{(+)}$ .

The scheme modifications for cases  $\Delta \geq -1$  (without range  $q < 0$ ) and  $q^* = 0$  (without range  $0 < q \leq q^*$ ) are straightforward.

**Note.** In summation  $Z^{(-)}$ , the care should be taken in managing overflow. The exponential index should not be limited by any value. Otherwise the relations between values of  $Z_1$  would be broken, making most probable momenta  $q < 0$  with nonequal energies  $(q - \omega/2\omega_c)^2$  to have similar weights.

Some way to avoid this, is to decrease the energy difference  $\delta E = E^{new} - E^{old} = 2q(q + \Delta)$  by some value into safe region.

- 
- [1] J.E. Hirsch, D.J. Scalapino, R.L. Sugar, and R. Blankenbecler, Phys. Rev. Lett. **47**, 1628 (1981).
  - [2] C. Lancsoz, J. Res. Nat. Bur. Stand. **45**, 244 (1950); E. Dagotto, Rev. Mod. Phys. **66**, No. 3, 763 (1994).
  - [3] N. Furukawa and M. Imada, J. Phys. Soc. Jpn. **60**, No. 3, 810 (1991).
  - [4] M. Ueda and A.J. Leggett, Phys. Rev. Lett. **83**, 1489 (1999).
  - [5] N.V. Prokof'ev, B.V. Svistunov, and I.S. Tupitsyn, Sov. Phys. JETP **87**, 310 (1998); N.V. Prokof'ev and B.V. Svistunov, Phys. Rev. Lett. **81**, 2514 (1998).
  - [6] N.V. Prokof'ev, B.V. Svistunov, and I.S. Tupitsyn, Phys. Lett. A **238**, 253 (1998).
  - [7] V.A. Kashurnikov, N.V. Prokof'ev, B.V. Svistunov, and I.S. Tupitsyn, Phys. Rev. B, **54**, 8644 (1996).
  - [8] Z. Néda and Z. Dezcö, cond-mat/9912383.
  - [9] M.H. Anderson *et al.*, Science **269**, 198 (1995); C.C. Bradley *et al.*, Phys. Rev. Lett. **75**, 1687 (1995); K.B. Davis *et al.*, Phys. Rev. Lett. **75**, 3969 (1995).
  - [10] G.P. Berman, A. Smerzi, and A.R. Bishop, Phys. Rev.

- Lett. **88**, 120402 (2002).
- [11] R.A. Duine and H.T.C. Stoof, Phys. Rev. Lett. **86**, 2204 (2001).
  - [12] Y. Castin and Ch. Herzog, Comptes Rendus de l'Academie des Sciences de Paris, tome 2, serie IV, pp. 419-443 (2001).
  - [13] G.B. Hess and W.M. Fairbank, Phys. Rev. Lett. **19**, 216 (1967).
  - [14] E.P. Gross, Nuovo Cimento, **20**, 454 (1961);
  - L.P. Pitaevskii, Sov. Phys. JETP **13**, 451 (1961).
  - [15] E.M. Lifshitz and L.P. Pitaevskii, *Statistical Physics, Part 2* (Vol. 9 of the *Course of Theoretical Physics* by L.D. Landau and E.M. Lifshitz), Pergamon Press, 1980.
  - [16] R. Kanamoto, H. Saito, and M. Ueda, cond-mat/0210229.
  - [17] J.B. McGuire, Jour. of Math. Phys. **5**, 622 (1964).
  - [18] H. Hasimoto, J. Fluid Mech. **51**, 477 (1972).